

# Optical-Resolution Photoacoustic Microscopy for Volumetric and Spectral Analysis of Histological and Immunochemical Samples\*\*

Yu Shrike Zhang, Junjie Yao, Chi Zhang, Lei Li, Lihong V. Wang,\* and Younan Xia\*

Dedicated to Professor George M. Whitesides on the occasion of his 75th birthday

**Abstract:** Optical-resolution photoacoustic microscopy (OR-PAM) is an imaging modality with superb penetration depth and excellent absorption contrast. Here we demonstrate, for the first time, that this technique can advance quantitative analysis of conventional chromogenic histochemistry. Because OR-PAM can quantify the absorption contrast at different wavelengths, it is feasible to spectrally resolve the specific biomolecules involved in a staining color. Furthermore, the tomographic capability of OR-PAM allows for noninvasive volumetric imaging of a thick sample without microtoming it. By immunostaining the sample with different chromogenic agents, we further demonstrated the ability of OR-PAM to resolve different types of cells in a coculture sample with imaging depths up to 1 mm. Taken together, the integration of OR-PAM with (immuno)histochemistry offers a simple and versatile technique with broad applications in cell biology, pathology, tissue engineering, and related biomedical studies.

As a technique for analyzing the microscopic anatomy of biological tissues, histology is typically performed by sectioning fixed tissues into thin slices with a microtome, followed by staining with chromogenic dyes and then examination under

an optical microscope. Although this technique has been serving biology and medicine as an invaluable tool for more than one century, there still remains room for improvement. For example, it is difficult to identify and quantify a specific component of interest in a histology image unless this component can be somehow singled out manually using specialized software. As a result, histology analysis is always labor-intensive and time-consuming. In addition, it is very challenging to generate a three-dimensional (3D) reconstruction of a sample during histology analysis.<sup>[1]</sup> With the help of confocal and multiphoton microscopy, it is now possible to perform 3D imaging and analysis but the samples have to be stained with fluorescent dyes that tend to be more susceptible to photobleaching than chromogenic dyes involved in histochemical staining. Because of the strong light scattering from biological tissues, the penetration depths of these optical imaging modalities are often limited to a few hundred micrometers.<sup>[2]</sup> The imaging depth further drops below 200  $\mu\text{m}$  when a highly scattering structure (e.g., a porous scaffold) is involved. Here we demonstrate that all these issues could be addressed by using optical-resolution photoacoustic microscopy (OR-PAM) to directly analyze the unstained samples, which is otherwise impossible with conventional optical microscopy.

As a newly developed technique, OR-PAM allows for noninvasive, volumetric imaging with relatively high spatial resolution and deep penetration.<sup>[3]</sup> In OR-PAM, a pulsed laser is focused and delivered into a biological sample to generate wide-band photoacoustic (PA) waves, which are collected using an ultrasonic transducer to generate an image (Figure S1 in the Supporting Information). OR-PAM can reach an imaging depth of ca. 1 mm while maintaining a lateral resolution of ca. 5  $\mu\text{m}$  and a depth resolution of ca. 15  $\mu\text{m}$ , both of which are on the same scale as individual cells and can be finely tuned by the bandwidth of the ultrasonic transducer.<sup>[4]</sup> Alternatively, optical sectioning of a few hundred nanometers can be achieved through nonlinear photoacoustic imaging.<sup>[5]</sup> To date, OR-PAM has found a wide spectrum of applications in biomedical research by working with intrinsic optical absorption contrast agents including hemoglobin, melanin, fluorescent proteins, and cytochromes,<sup>[6,7]</sup> or external contrast agents such as indocyanine green (ICG), carbon nanotubes, and metal nanoparticles.<sup>[6,8]</sup> As recently demonstrated by our groups, the capability of OR-PAM could be extended to image essentially all types of living cells by staining them with a metabolic dye.<sup>[9]</sup> Here we further establish that OR-PAM can also be used for volumetric and spectral examination of histological samples with

[\*] Dr. Y. S. Zhang,<sup>[†]</sup> Prof. Y. Xia  
 The Wallace H. Coulter Department of Biomedical Engineering  
 Georgia Institute of Technology and Emory University  
 Atlanta, GA 30332 (USA)  
 E-mail: younan.xia@bme.gatech.edu  
 Prof. Y. Xia  
 School of Chemistry and Biochemistry  
 Georgia Institute of Technology  
 Atlanta, GA 30332 (USA)  
 Dr. J. Yao,<sup>[†]</sup> C. Zhang, L. Li, Prof. L. V. Wang  
 Department of Biomedical Engineering  
 Washington University in St. Louis  
 St. Louis, MO 63130 (USA)  
 E-mail: lhwang@biomed.wustl.edu

[†] These authors contributed equally to this work.

[\*\*] This work was supported by NIH grants DP1 OD000798 (NIH Director's Pioneer Award) to Y.X., and DP1 EB016986 (NIH Director's Pioneer Award), R01 CA186567 (NIH Director's Transformative Research Award), and R01 CA159959 to L.V.W. L.V.W. has a financial interest in Endra, Inc., and Microphotoacoustics, Inc., which did not support this work. Part of the research was performed at the Alafi Neuroimaging Laboratory, the Hope Center for Neurological Disorders in Washington University School of Medicine, which is supported by the NIH Neuroscience Blueprint Center Core Grant P30 NS057105.



Supporting information for this article is available on the WWW under <http://dx.doi.org/10.1002/anie.201403812>.

a minimum effort for either sample preparation or image analysis.

We first demonstrated the feasibility of using OR-PAM to directly analyze the samples stained by the traditional histological dyes. Figure 1a shows a representative transmission optical micrograph of a mouse connective tissue slice (ca. 5  $\mu\text{m}$  thick) stained with Masson's trichrome, where the erythrocytes, cytoplasm, and collagen fibrils were bright red, pinkish purple, and blue, respectively. From this optical micrograph, however, it was very difficult to single out a specific component for further analysis. In contrast, by using OR-PAM and taking advantage of the unique absorption spectrum of each dye, the different components could be

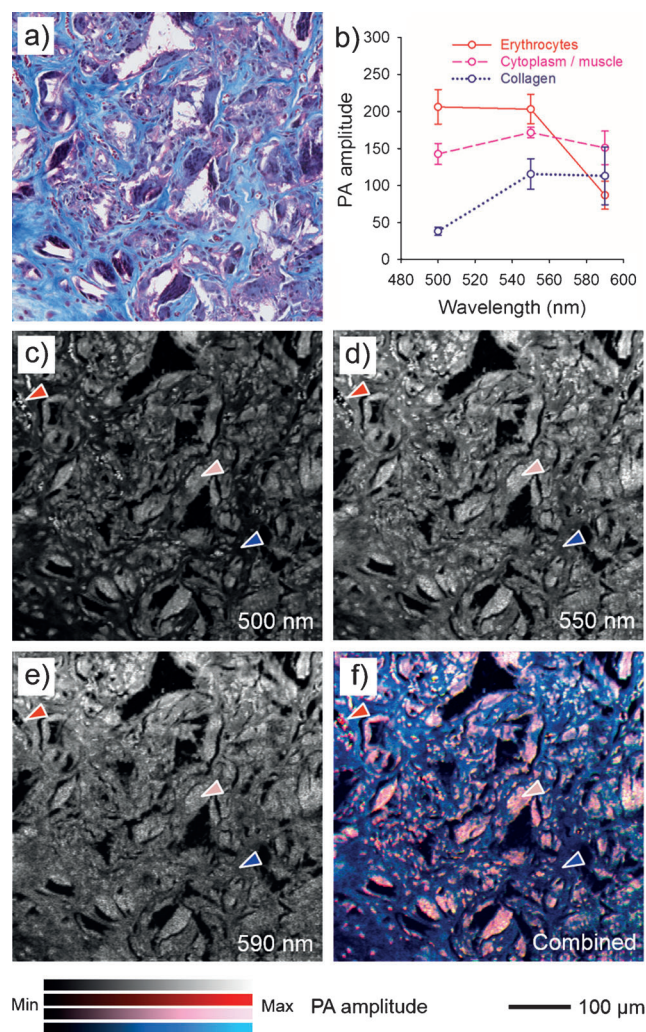


**Figure 1.** a) A transmission optical micrograph of a histological slice of 5  $\mu\text{m}$  thick that was sectioned from mouse connective tissue and stained with Masson's trichrome. The erythrocytes, cytoplasm, and collagen were stained bright red, pinkish purple, and blue, respectively. b) PA signals collected from the aforementioned three components at wavelengths of 500 nm, 550 nm, and 590 nm. c–e) OR-PAM MAP images of the same sample acquired at wavelengths of 500 nm, 550 nm, and 590 nm, respectively. The arrowheads with three different colors indicate representative components of erythrocytes, cytoplasm, and collagen. f) Combined OR-PAM MAP image of the three components that were spectrally decomposed. The same features could be observed as in (a). MAP: maximum amplitude projection.

readily separated from each other. As shown in Figure 1b, the PA signals from the stained erythrocytes decreased remarkably when the laser wavelength was tuned from 500 to 550 and then 590 nm. In comparison, the stained collagen showed an opposite trend, with weak PA signals at 500 nm but much stronger PA signals at 550 nm and 590 nm. The stained cytoplasm showed relatively uniform PA amplitudes at all wavelengths. Figure 1c–e, shows OR-PAM maximum amplitude projection (MAP) images of the same sample acquired at 500, 550, and 590 nm, respectively. Three sets of arrowheads with different colors were used to indicate the erythrocytes, cytoplasm, and collagen at the same locations. At 500 nm, erythrocytes gave the strongest PA signals, followed by cytoplasm, while collagen was barely detectable (Figure 1c). At 550 nm, all the three components showed similar PA amplitudes (Figure 1d). The erythrocytes were not detectable at 590 nm (Figure 1e). As shown in Figure 1f, all three components could be easily differentiated in a combined PAM MAP image after spectral analysis. It should be pointed out that the superimposed PAM MAP image in Figure 1f might suffer a certain degree of loss in details as compared to Figure 1a. This issue can be addressed by taking PAM images with a greater signal-to-noise ratio to obtain more accurate spectral analysis, or using imaging systems with higher lateral resolutions.<sup>[5,10]</sup> Based on the PAM data, we could further quantify the area occupied by each component. In Figure 1f, the areas occupied by erythrocytes, cytoplasm, and collagen were 5717, 90097, and 134190  $\mu\text{m}^2$ , respectively, corresponding to a ratio of roughly 1:16:24. These results demonstrate that OR-PAM can significantly reduce the amount of time required for image analysis while ensuring a desired quality for the image. The same strategy is also applicable to other histological staining with multiple colors, including the hematoxylin and eosin staining that gives cytoplasm and nuclei pinkish red and blue colors, respectively. As shown in Figure S1a, eosin has a sharp absorption peak at ca. 520 nm whereas hematoxylin shows a broad peak extending from < 400 nm all the way to 650 nm. Accordingly, using a dual-wavelength PAM at 523 nm and 587 nm, we could effectively differentiate the hematoxylin-stained nuclei from the eosin-stained cytoplasm in the same image (Figure S1c–e).

In addition to traditional histology, we further extended OR-PAM to immunostaining in an effort to achieve better selectivity. Figure 2a shows the UV/Vis spectrum of the reaction product of horseradish peroxidase (HRP) and ImmPACT diaminobenzidine (DAB) peroxidase substrate, which has a strong absorption peak at 320 nm, in addition to a broad peak extending from ca. 400 nm to 900 nm. Figure 2b shows a transmission optical micrograph of MC3T3 preosteoblasts whose f-actin was labeled in sequence with biotin-phalloidin and streptavidin-HRP, followed by color development with DAB. Figure 2c shows an OR-PAM MAP image captured at 570 nm from a different region of the same sample, clearly revealing both the stained cytoskeleton and unstained nuclei. This result demonstrates the ability of OR-PAM to resolve the specific components of a cell after immunostaining.

We then seeded MC3T3 preosteoblasts in a poly(D,L-lactide-co-glycolide) (PLGA) inverse opal scaffold with uni-

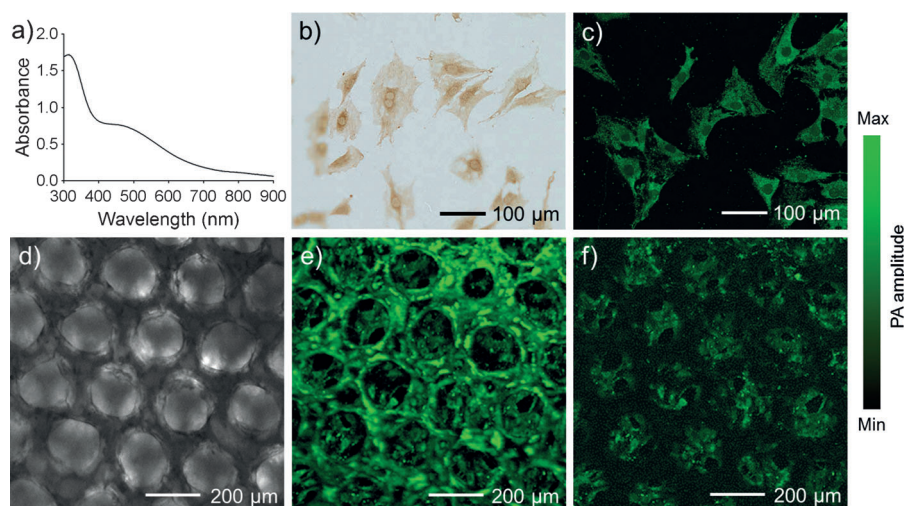


**Figure 2.** a) UV/Vis absorption spectrum of the reaction product of ImmPACT DAB and horseradish peroxidase (HRP). b) A transmission optical micrograph of MC3T3 cells stained for f-actin in sequence with biotin-phalloidin, streptavidin-HRP, and DAB. c) Submicron high-resolution OR-PAM MAP image showing MC3T3 cells stained for f-actin with the same procedure as in (b). d) A transmission optical micrograph showing the cells cultured in an inverse opal scaffold for three days and stained with biotin-phalloidin/HRP-streptavidin/DAB. e) OR-PAM MAP image of the same cell/scaffold construct in (d). f) OR-PAM image showing the bottom section (100–200  $\mu\text{m}$  beneath the top surface) of the surface pores in the scaffold. Note that cell attachment and the structure of the pores can be clearly observed.

form pores.<sup>[6d,7e,i,8h,9,11]</sup> Figure 2d shows a transmission optical micrograph of cells that were cultured in the scaffold for 3 days and then stained for f-actin in sequence with biotin-phalloidin, streptavidin-HRP, and DAB. The cells typically stretched along the walls of the pores. As shown in the OR-PAM MAP image (Figure 2e), the same pattern of cell attachment was also observed. In addition, we could resolve the 3D distribution of the stained cells in the scaffold (Movie S1). We noticed that the cells at 100–200  $\mu\text{m}$  below the top surface of the scaffold also showed up in the MAP image (Figure 2e) and the PA signals from these cells could be easily separated from the rest of the sample (Figure 2f) based on the volumetric information provided by PAM. In comparison, it was very difficult to resolve these cells under a transmission optical microscope (Figure 2d) unless the scaffold can be physically sectioned into thin slices prior to imaging. Owing to the one-way optical scattering and the much weaker return acoustic scattering by the sample during imaging, OR-PAM can easily reach a penetration depth of 200–300  $\mu\text{m}$  for such scaffold-based samples, which is more than twice that of confocal microscopy. The penetration depth can be further doubled by imaging the sample from both the top and bottom sides.<sup>[12]</sup> At the expense of spatial resolution, PA imaging can even achieve a penetration depth on the scale of centimeters.<sup>[13]</sup> Furthermore, PA imaging is essentially background-free because OR-PAM relies on optical absorption and therefore cells, cellular components, extracellular matrix (ECM) molecules, and biomaterials with no absorption at the laser wavelength should not contribute to the PA signals. This important feature of PAM holds its superiority to fluorescence-based imaging modalities (e.g., confocal and multiphoton microscopy) especially for observing tissue-level

samples because certain ECM molecules (or scaffolds) such as collagen can give strong autofluorescence over a broad range of wavelengths, greatly limiting the selection of fluorescent dyes.<sup>[14]</sup>

OR-PAM can also be used to differentiate cells enhanced by chromogenic immunostaining. This capability is made possible by the recent development of various chromogenic substrates that present distinctive absorption spectra after reacting with HRP, including ImmPACT DAB (brown), NovaRed (red), and Vector SG (blue/gray).<sup>[15]</sup> In our study, we chose ImmPACT DAB and NovaRed because the absorption spectra of their reaction products with HRP match the wavelengths currently used in our PAM. Figure 3a shows the absorption spectra of reaction products of HRP with ImmPACT DAB and NovaRed, respectively. The product of DAB chromogen had a distinct absorption peak at ca. 500 nm, whereas both

products showed similar absorptions at  $> 570$  nm. The photographs in the inset of Figure 3a clearly show the different colors of the two chromogenic products. We attempted to distinguish cell populations in a sample co-cultured from MC3T3 preosteoblasts and SK-BR-3 human breast tumor cells. Figure 3b shows a typical reflection optical micrograph of the sample supported on a glass slide. The f-actins of both types of cells were stained consecutively with biotin-phalloidin, streptavidin-HRP, and DAB (brown), whereas the SK-BR-3 cells were further stained in sequence with anti-HER2 primary antibody (specific to human), HRP-secondary antibody, and NovaRed (dark red) for HER2 antigens on their surfaces. Unlike MC3T3 cells that assumed highly stretched shapes with large areas, SK-BR-3 cells were characterized by their relatively small sizes and less stretched shapes. Figure 3c shows another transmission optical micrograph taken from a sample co-cultured in a PLGA inverse opal scaffold with a uniform pore size of 200  $\mu\text{m}$ . The sample was then imaged by OR-PAM at dual wavelengths of 523 nm and 570 nm. Based on the absorption spectra of the two dyes, SK-BR-3 cells could be spectrally unmixed from the background MC3T3 cells using custom-coded MATLAB programs (Figure 3d, where SK-BR-3 cells are shown in yellow/green and MC3T3 cells in reddish brown). Movie S2 shows volumetric rendering of the two cell populations in the scaffold. The exact locations of the SK-BR-3 cells could be determined in magnified PAM MAP images from topical and sagittal views (Figure 3e). Volumetric distributions of individual SK-BR-3 cells or their clusters could be clearly resolved across the entire thickness of the scaffold, which was filled with MC3T3 cells (Figure 3c).

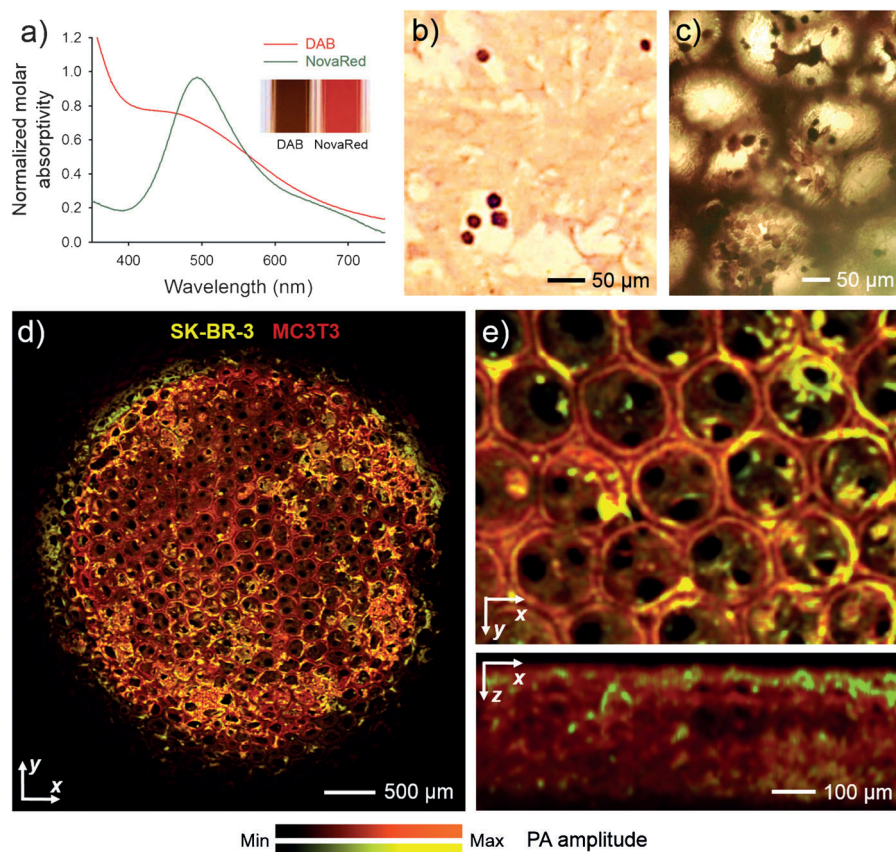


**Figure 3.** a) Normalized molar absorptivity of the reaction products of HRP with DAB and NovaRed, respectively. The inset displays optical micrographs of these products, clearly showing their different colors. b) An optical micrograph of a co-culture sample of SK-BR-3 and MC3T3 cells on a glass slide after staining with biotin-phalloidin/streptavidin-HRP/DAB for f-actin, and anti-HER2/HRP-secondary antibody/NovaRed for HER2 antigens on the surfaces of SK-BR-3 cells. The SK-BR-3 cells were shown in red while the MC3T3 cells in the background were shown in brown. c) An optical micrograph showing a 7 day co-culture sample in a PLGA inverse opal scaffold obtained by following the same staining procedure as in (b). d) OR-PAM MAP image of the same scaffold at a low magnification, where SK-BR-3 and MC3T3 cells could be digitally separated in the image using a custom-written spectral unmixing algorithm (see the Supporting Information for details). e) Magnified views of the same sample showing volumetric distribution of the two cell types from the top and side, respectively.

In summary, we have successfully demonstrated the superior performance of OR-PAM in analyzing histology samples in both two and three dimensions. Biological components stained with traditional chromogenic histological dyes can be spectrally separated in PAM imaging. In addition, we have shown that OR-PAM can image specific cell-markers-stained immunohistochemistry. More importantly, volumetric information can be directly obtained using OR-PAM without physically sectioning, although the protocols for staining three-dimensional samples with chromogenic histochemistry still need to be optimized.<sup>[16]</sup> Taken together, we expect that OR-PAM will become a potent alternative imaging technique for histology analysis in applications including cell biology, pathology, tissue engineering, and regenerative medicine.

Received: March 28, 2014  
Published online: June 24, 2014

**Keywords:** biomedical imaging · cell biology · histochemistry · photoacoustic microscopy · tissue engineering

- [1] Y. Song, D. Treanor, A. J. Bulpitt, D. R. Magee, *J. Pathol. Inform.* **2013**, 4, 7.
- [2] D. Dumas, B. Riquelme, E. Werkmeister, N. D. Isla, J. F. Stoltz, *Multimodality of Microscopy Imaging Applied to Cartilage Tissue Engineering*, IOS Press, Amsterdam, **2007**.
- [3] a) K. Maslov, H. F. Zhang, S. Hu, L. V. Wang, *Opt. Lett.* **2008**, 33, 929–931; b) S. Hu, K. Maslov, L. V. Wang, *Opt. Lett.* **2011**, 36, 1134–1136.
- [4] C. Zhang, K. Maslov, J. Yao, L. V. Wang, *J. Biomed. Opt.* **2012**, 17, 116016.
- [5] J. Yao, L. Wang, C. Li, C. Zhang, L. V. Wang, *Phys. Rev. Lett.* **2014**, 112, 014302.
- [6] a) L. V. Wang, *Nat. Photonics* **2009**, 3, 503–509; b) L. V. Wang, S. Hu, *Science* **2012**, 335, 1458–1462; c) C. Kim, C. Favazza, L. V. Wang, *Chem. Rev.* **2010**, 110, 2756–2782; d) X. Cai, Y. S. Zhang, Y. Xia, L. V. Wang, *Mater. Today* **2013**, 16, 67–77.
- [7] a) H. F. Zhang, K. Maslov, M. Sivaramakrishnan, G. Stoica, L. V. Wang, *Appl. Phys. Lett.* **2007**, 90, 053901; b) L. Li, R. J. Zemp, G. Lungu, G. Stoica, L. V. Wang, *J. Biomed. Opt.* **2007**, 12, 020504; c) D. Razansky, M. Distel, C. Vinegoni, R. Ma, N. Perriimon, R. W. Koster, V. Ntziachristos, *Nat. Photonics* **2009**, 3, 412–417; d) D.-K. Yao, K. Maslov, K. K. Shung, Q. Zhou, L. V. Wang, *Opt. Lett.* **2010**, 35, 4139–4141; e) Y. Zhang, X. Cai, S. W. Choi, C. Kim, L. V. Wang, Y. Xia, *Biomaterials* **2010**, 31, 8651–8658; f) A. Krumholz, S. J. Vanvickle-Chavez, J. Yao, T. P. Fleming, W. E. Gilanders, L. V. Wang, *J. Biomed. Opt.* **2011**, 16, 080503; g) Y. Wang, S. Hu, K. Maslov, Y. Zhang, Y. Xia, L. V. Wang, *Opt. Lett.* **2011**, 36, 1029; h) J. Yao, K. I. Maslov, Y. Zhang, Y. Xia, L. V. Wang, *J. Biomed. Opt.* **2011**, 16, 076003–076011; i) X. Cai, Y. Zhang, L. Li, S. W. Choi, M. R. MacEwan, J. Yao, C. Kim, Y. Xia, L. V. Wang, *Tissue Eng.* **2012**, 19, 196–204; j) X. Cai, L. Li, A. Krumholz, Z. Guo, T. N. Erpelding, C. Zhang, Y. Zhang, Y. Xia, L. V. Wang, *PlosONE* **2012**, 7, e43999; k) G. S. Filonov, A. Krumholz, J. Xia, J. Yao, L. V. Wang, V. V. Verkhusha, *Angew. Chem.* **2012**, 124, 1477–1480; *Angew. Chem. Int. Ed.* **2012**, 51, 1448–1451; l) C. Zhang, Y. S. Zhang, D. K. Yao, Y. Xia, L. V. Wang, *J. Biomed. Opt.* **2013**, 18, 020504.
- [8] a) S. Mallidi, T. Larson, J. Tam, P. P. Joshi, A. Karpouk, K. Sokolov, S. Emelianov, *Nano Lett.* **2009**, 9, 2825–2831; b) Y. Jin, C. Jia, S. W. Huang, M. O'Donnell, X. Gao, *Nat. Commun.* **2010**, 1, 41; c) C. Kim, E. C. Cho, J. Chen, K. H. Song, L. Au, C. Favazza, Q. Zhang, C. M. Cobley, F. Gao, Y. Xia, L. V. Wang, *ACS Nano* **2010**, 4, 4559–4564; d) X. Cai, W. Li, C. H. Kim, Y. Yuan, L. V. Wang, Y. Xia, *ACS Nano* **2011**, 5, 9658–9667; e) C. Li, C. Zhang, L. Gao, A. Garcia-Urbe, L. V. Wang, *J. Biomed.*

- Opt.* **2013**, *18*, 106004; f) Y. S. Zhang, Y. Wang, L. Wang, Y. Wang, X. Cai, C. Zhang, L. V. Wang, Y. Xia, *Theranostics* **2013**, *3*, 532–543; g) Y. S. Zhang, X. Cai, J. Yao, W. Xing, L. V. Wang, Y. Xia, *Angew. Chem.* **2014**, *126*, 188–192; *Angew. Chem. Int. Ed.* **2014**, *53*, 184–188.
- [9] Y. Zhang, X. Cai, Y. Wang, C. Zhang, L. Li, S.-W. Choi, L. V. Wang, Y. Xia, *Angew. Chem.* **2011**, *123*, 7497–7501; *Angew. Chem. Int. Ed.* **2011**, *50*, 7359–7363.
- [10] a) C. Zhang, K. I. Maslov, L. V. Wang, *Opt. Lett.* **2010**, *35*, 3195–3197; b) C. Zhang, Y.-J. Cheng, J. Chen, S. Wickline, L. V. Wang, *J. Biomed. Opt.* **2012**, *17*, 020501.
- [11] a) S.-W. Choi, Y. Zhang, S. Thomopoulos, Y. Xia, *Langmuir* **2010**, *26*, 12126–12131; b) S.-W. Choi, Y. Zhang, Y. Xia, *Langmuir* **2010**, *26*, 19001–19006; c) Y. Zhang, S.-W. Choi, Y. Xia, *Macromol. Rapid Commun.* **2012**, *33*, 296–301; d) S.-W. Choi, Y. Zhang, M. R. MacEwan, Y. Xia, *Adv. Healthcare Mater.* **2013**, *2*, 145–154; e) Y. S. Zhang, K. P. Regan, Y. Xia, *Macromol. Rapid Commun.* **2013**, *34*, 485–491; f) Y. S. Zhang, S. W. Choi, Y. Xia, *Soft Matter* **2013**, *9*, 9747–9754.
- [12] J. Yao, K. I. Maslov, E. R. Puckett, K. J. Rowland, B. W. Warner, L. V. Wang, *Opt. Lett.* **2012**, *37*, 659–661.
- [13] a) G. Ku, L. V. Wang, *Opt. Lett.* **2005**, *30*, 507–509; b) C. Kim, T. N. Erpelding, L. Jankovic, M. D. Pashley, L. V. Wang, *Biomed. Opt. Express* **2010**, *1*, 278–284.
- [14] a) D. S. Gareau, P. R. Bargo, W. A. Horton, S. L. Jacques, *J. Biomed. Opt.* **2004**, *9*, 254–258; b) J. R. Mansfield, K. W. Gossage, C. C. Hoyt, R. M. Levenson, *J. Biomed. Opt.* **2005**, *10*, 041207.
- [15] *Discovery through Color. A Guide to Multiple Antigen Labeling*, Vector Laboratories, Burlingame, **2005**.
- [16] K. Chung, J. Wallace, S. Y. Kim, S. Kalyanasundaram, A. S. Andalman, T. J. Davidson, J. J. Mirzabekov, K. A. Zalocusky, J. Mattis, A. K. Denisin, S. Park, H. Bernstein, C. Ramakrishnan, L. Grosenick, V. Gradinaru, K. Deisseroth, *Nature* **2013**, *497*, 332–337.